Effect of In0.70Ga0.30As quantum dot insertion in the middle cell of InyGa1-yP/InxGa1-xAs/Ge triple-junction for solar cells

Abdelkader Aissat, Said Nacer, Jean-Pierre Vilcot

Effect of $In_{0.70}Ga_{0.30}As$ Quantum Dot Insertion in the Middle Cell of $In_yGa_{1-y}P/In_xGa_{1-x}As$/Ge Triple-Junction for Solar Cells

A. Aissat[1,2,*], S.Nacer[1], J.P.Vilcot[2]
[1]Faculty of Technology, University of Blida.1, 09000, Blida, Algeria
[2]Institute of Electronics, Microelectronics and Nanotechnology (IEMN), UMR CNRS 8520.
University of Lille Avenue Poincaré, CS 60069,
59652 Villeneuve d'Ascq cedex, France
email : sakre23@yahoo.fr

Abstract

This paper focuses on the simulation and optimization of electrical and structural properties of high efficiency InGaP/InGaAs/Ge triple junction solar cells that incorporate $In_{0.7}Ga_{0.3}As$ quantum dots with in the GaAs middle cell material. Current density-voltage (J-V), external quantum efficiency (EQE) and capacitance-voltage (C-V) characteristics have been simulated and discussed. Results show that 30 pairs of $In_{0.70}Ga_{0.30}As$ (QD)/GaAs (barrier) in the middle cell provide a relative enhancement of 13 % in EQE in the 900-1000 nm wavelength range. This leads to a short-circuit current of 20 mA/cm^2, an open circuit voltage of 2.3 V, a fill factor of 81.73 %, and a conversion efficiency of 39.03 %. The C-V revealed that a relatively high number of interfacial states are present in the 3-J cell structure including the QD layers, which decreases the open circuit voltage. In this study we benefited 18% of relative efficiency.

Keywords: New Materials; Quantum Dot; Solar Cell; Optoelectonic.

1. INTRODUCTION

Several researchers in the photovoltaic field aim to find materials and advanced reliable technologies to produce high efficiency, low-cost solar cells [1,2,3]. Others use nanostructures like nanowires to increase the cell solar absorption coefficient [4,5].

Among the numerous technologies used to improve the conversion efficiency of solar cells, the multi-junction (M-J) concept, especially the triple-junction (3-J) concept based on InGaP, GaAs and Ge materials exhibit high efficiencies [6]. Nevertheless, their performance is somehow restricted due to current limitation of the GaAs middle cell and lattice mismatch of Ge substrate. Many approaches have been proposed to overcome those limitations and enhance the conversion efficiency of the 3-J configurations. The first approach consists in inserting a fourth subcell with a bandgap energy about 1 eV in order to absorb the photons which have a bandgap energy between 1.42 eV (GaAs) and 0.67 eV (Ge). InGaAsN is then a good candidate thanks to its lattice matched to Ge substrate and to its tunable bandgap energy. Theoretical calculations have indicated that such structures provide a conversion efficiency of about 47.7 % [7, 8]. The second approach consists of inserting an intermediate band in the 3-J structure [9]. Aim is then to improve the spectral response of the solar cell in the energy region below the absorption edge of host material. Luque et al have been the first who proposed to insert multiple layers of InAs quantum dots (QDs) in GaAs subcell as an intermediate band [9]. Currently, two material systems are being studied: InGaAs/GaAs quantum wells (QWs) [10-12] and InAs/InGaAs QD materials [13-18]. Otherwise, the growth of multiple layers of QD and QW is a technological challenge. Quantum dots have several applications in different fields such as microelectronics, quantum processing, and optoelectronic devices [19].

The accumulation of stress during epitaxial growth tends to generate dislocations and defects affecting the crystalline quality of the layers and resulting in a lack of uniformity [20]. To overcome those problems, the growth of strain compensation layers using the indium flash techniques have been demonstrated [21,22].

In this study, InGaP/InGaAs/Ge 3-J cell structure without and with $In_{0.70}Ga_{0.30}As$ (QD)/GaAs (barrier) periods in the InGaAs middle cell is modeled, simulated and optimized. In order to

increase the electrons carrier's confinement in the quantum dots, we fixed the concentration indium y=70% with a bandgap E_g = 0.54eV. So, we got an electron confinement rate around 88%. Our objective is to insert the maximum of quantum dots to carry out intermediate bands energy in order to absorb the photons which have an energy lower than the bandgap ($E_{photon} < E_g$). Already the efficiency of the 3-J structure increases considerably compared to a single solar cell. The creation of intermediate energy bands causes a more significant increase than a 3-J solar cell.

2. THEORETICAL MODEL

The following section describes the physical models and empirical equations that have been used for this simulation. The current supplied by a Quantum Dot Solar Cell is the sum of the photocurrents issued in both the bulk and QDs regions. To calculate this current, Poisson and Schrödinger equations are numerically coupled and solved as detailed in ref. [23,24]. Details on the variation of mobility with carrier concentration that is described by Masetti model and on the SRH recombination model that uses concentration dependent lifetimes are given in ref. [25]. We note here that we have neglected the radiative recombination since our simulations are done for room temperature [26].

The self-consistent 1D coupled Schrödinger Poisson model for electrons and holes express then respectively by the following equations [27]:

$$\frac{-h^2}{2}\frac{\partial}{\partial z}\left(\frac{1}{m_e^*(z)}\frac{\partial \psi_i}{\partial z}\right) = (E_{ne} - E_c(z))\psi_i \quad (1)$$

$$\frac{-h^2}{2}\frac{\partial}{\partial z}\left(\frac{1}{m_h^*(z)}\frac{\partial \psi_i}{\partial z}\right) = (E_{nh} - E_h(z))\psi_i \quad (2)$$

where E_c (z) and E_h (z) are the conduction and valence band edge, respectively, and m_e* and m_h* the electron and hole effective mass, respectively. ψ_i, E_{ne} , E_{nh} are the wavefunction and energy level of subband.

The EQE of p and n-regions of the top and bottom subcells is classically evaluated by solving the carrier transport equations described by drift-diffusion model presented in ref. [24,28].

The EQE of the photogenerated carriers in the middle subcell which contains the QDs periods is calculated by [28-30].

$$EQE(\lambda) = \big(1 - R(\lambda)\big)\big[1 - \exp -\big(\alpha_B L + N_{QD}\alpha^*_{QD}\big)\big].\exp(-\textstyle\sum_1^n \alpha_i\, z_i)\,, \quad n = 1\,, 2, 3\,\ldots \qquad (3)$$

$$\alpha^*_{QD}(E) = \delta.\big[\textstyle\sum_{m,n}\alpha_{en-hh_m}(E) + \sum_{m,n}\alpha_{en-lh_m}(E)\big]$$

(4)

In this structure we took into account the antireflection layer, emitting layer and the space charge region of the emitting layer. The second exponential factor present the light attenuation in the layers between the cell surface and the depletion layer [29]. The parameters α_i and z_i are the absorption coefficient and the width of these precedent layers, respectively, α_B is the absorption coefficient of the bulk barrier material. L is the length of intrinsic region, α^*_{QD} is the dimension less quantum dot absorption coefficient, used for energies below the barrier bandgap, N_{QD} is the quantum dots number.

R(λ) is the surface reflectivity that have been set to a constant value of 0.1, α_{en-hh_m} and α_{en-lh_m} are the absorption coefficients due to electron-heavy hole and electron-light hole valence to conduction band, respectively, δ is the quantum thickness of the heterostructure [29, 30]. The absorption coefficient for the transitions between electron heavy hole and light hole minibands as a function of their widths, $\gamma_{hh,lh}$ and γ_e [31,32]

$$\alpha_{en-hh_m,lh_m}(E) = B|\langle f|c.p|i\rangle|^2.m_{r\ hh,lh}\left\{0.5 + \frac{1}{\pi}\ arcsin\left[\frac{E - E_{T\,e-hh,lh} - \gamma_{hh,lh}}{\gamma_{hh,lh}}\right]\right\} \qquad (5)$$

$$m_{r\ hh,lh} = \frac{m_e + m_{hh,lh}}{m_e.m_{hh,lh}} \qquad (6)$$

$$\gamma_{hh,lh} = \frac{1}{2}\big(\gamma_e + \gamma_{hh,lh}\big) \qquad (7)$$

$$B = \frac{q^2}{2\pi f m_e^2 \varepsilon_0 \hbar^2 n_r d_{sl} c} \qquad (8)$$

where $\langle f|c.p|i\rangle$ is the matrix element between the initial *i* and the final *f* states.

f is the frequency.

n_r is the relative refraction index of heterostructure.

c is a unit vector in the propagation direction.

p is a differential operator.

m_e is the effective mass of electron

$m_{hh,lh}$ are the effective mass of heavy hole and light hole.

ε_0 is the vacuum dielectric constant.

$\gamma_{hh,lh}$ is the width of the heavy hole and light hole band.

c is the speed of light in a vacuum.

d_{sl} is the cluster width.

To calculate the absorption coefficient of the direct bandgap materials constituting the 3-J cell, the Urbach equation was used [33].

$$\alpha(\lambda) = \alpha_0 \sqrt{\frac{1.24}{\lambda} - E_g(x,T)}$$

(9)

where α_0 is the optical wave energy function constant of a semiconductor. λ is the wavelength.

The bandgap energy of the materials is determined by the following expression:

$$E_g = \begin{cases} E_{In(x)Ga(1-x)As} = xE_{g\ InAs} + (1-x)E_{g\ GaAs} - bx(1-x) \\ E_{In(y)Ga(1-y)P} = yE_{g\ InP} + (1-y)E_{g\ GaP} - cy(1-y) \end{cases}$$

(10)

With b, c are the Bowing parameters.

The parameters of the relative permittivity are given par the following equation:

$$\varepsilon_r = \begin{cases} \varepsilon_{r\ In(x)Ga(1-x)As} = x.\varepsilon_{r\ InAs} + x(1-x)\varepsilon_{r\ GaAs} + dx(1-x) \\ \varepsilon_{r\ In(y)Ga(1-y)P} = y.\varepsilon_{r\ InAs} + y(1-y)\varepsilon_{r\ GaAs} + ey(1-y) \end{cases} \quad (11)$$

Where d, e are the Bowing parameters.

The parameters used in this study are listed in Table I [34,35].

The photocurrent density J_{ph} is determined from the convoluted incident spectrum with the external quantum efficiency of the cell. The carrier transport equations have been solved

within minority carrier diffusion and depletion approximations at T=300K, [36,29] to determine the effect of p and n-doped regions on external quantum efficiency by taking into account the absorption of excitons in order to have an exact correspondence with experiment in the long wavelength region [37]. The exciton binding energies have been analytically determined within the framework of fractional-dimensional space [37]. When the total EQE is obtained the photocurrent density can be calculated by integration [29]:

:

$$J_{ph} = q \int_{\lambda_i}^{\lambda_f} EQE(\lambda).\phi(\lambda)d\lambda$$

(12)

where λ_i is initial wavelength and λ_f is the final wavelength of the solar spectrum, $\phi(\lambda)$ is spectral solar irradiance AM1.5.

The capacitance as function of the forward voltage is calculated using the following equation:

$$C = \frac{1}{2\pi fV}.J_{ph}$$

(13)

With f is the frequency of the forward voltage applied; V is the forward voltage applied.

In order to examine the recombination in the 3-J solar cell with and without the QD layers, the capacitance was estimated using the following equation [25].

$$\frac{1}{C^2} = \frac{2}{qA^2\varepsilon_0\varepsilon_r N}\cdot\left(V_{bi} - V_{bias} + \frac{K_B T}{q}\right)$$

(14)

where

V_{bi} is the built-in potential.

V_{bias} is the bias voltage.

A is the junction area.

ε_0, ε_r are the vacuum and relative permittivity, respectively.

N is the activated dopant density in the semiconductor.

T is the temperature.

K_B is the Boltzmann's constant.

q is the electron charge.

2. RESULTS AND DISCUSSION

Fig.1 presents a schematic diagram of InGaP/InGaAs/Ge 3-J structure comprising an InGaP top cell, GaInAs middle cell, and a Ge bottom cell. In Fig.2 (a,b) a number of quantum dots $In_{0.70}Ga_{0.30}As$ (QD)/GaAs (barrier) layer are implanted in the intrinsic region of InGaAs middle cell with a dot size of d=5 nm and L=10 nm . Table II summarizes the parameters of each layer of InGaP/InGaAs/Ge 3-J [7].

First, we investigated a triple junction solar cell based on InGaP/InGaAs/Ge. Fig.3 shows the evolution of the current density as a function of the voltage of a multi-junction solar cell based on three $In_yGa_{1-y}P/In_xGa_{1-x}As$/Ge semiconductors. In this study, we have optimized the structure $In_{0.60}Ga_{0.40}P/In_{0.17}Ga_{0.83}As$/Ge. For a concentration of indium x=17% in the InGaAs structure, the energy of the band gap is E_g = 1.132eV. For the InGaP structure, the indium concentration is y = 60% with a bandgap energy E_g = 1.738eV.

It is noted that the open circuit voltage V_{oc} of the total cell achieved 2.35V and the density of the current J_{SC} does not exceed the 15.30 mA/cm^2 value. The open circuit voltage of the total cell is equal to the sum of the three voltages of each single solar cell. On the other hand, the current density tends towards that of the solar cell which has the low current density. Fig .4 illustrates the variation of the power density of each single cell and the total cell as a function of the voltage. Note that the power density of the total solar cell is important. It reaches the value of 31.84mW/cm^2, this increase has a positive effect on the total efficiency.

Secondly, we have chosen an AM1.5G solar spectrum illumination and a cell temperature of T=300 K. We start the simulation of the InGaP/InGaAs/Ge 3-J solar cell structure for different numbers of QDs layers inserted in the middle cell (0, 10, 20, and 30), respectively. For each

simulation, the current-voltage characteristic J-V, the external quantum efficiency EQE and the characteristic properties of the solar cell are calculated. Secondly, we investigated the capacitance-voltage C-V of 3-J with and without QDs layers in order to examine the crystal quality and interfacial states of the structures. The drift-diffusion, Poisson, Schrödinger equations, described above are coupled and solved numerically for J-V and EQE characteristics at all mesh points of the device. Eq.6 is employed to plot the C-V characteristic. The physical parameters of the materials used in this simulation are extracted from [38,39].

The EQE spectra of the InGaAs middle cell where the QDs layers are embedded. Fig. 5 represents EQE as a function of wavelength considering no or 30 QDs layers inserted. Both structures present a maximum value of EQE in the 650 nm-850 nm wavelength range. This maximal value is nevertheless smaller for the cell including QDs. One possible explanation can be linked to the insertion of the QDs layers that causes a degradation of the material properties under a higher strain in the films. However, it was observed that the EQE of 3-J cell without QDs turns to zero around the wavelength 875 nm. Thus, the photons with energy lower than GaAs bandgap energy cannot be absorbed. Otherwise, longer wavelengths (>875 nm) are absorbed by the QDs layers inserted leading to the generation of an extra current. The insertion of QDs layers red-shifts the absorption edge of InGaAs cell by roughly 100 nm with an enhancement of about 13% in EQE obtained in the 900-1000 nm wavelength range.

Fig. 6 represents the current density-voltage J-V of the InGaP/InGaAs/Ge 3-J without and with QDs layers.10, 20 and 30 layers have been modeled. The effect of QDs number on J_{sc} is remarkable. For 30xQDs the J_{sc} tend towards the value 20mA/cm^2. From 30xQDs the J_{sc} is saturated. The increase in the QDs number causes a reduction in V_{oc}.

Table III summarizes all the solar cell characteristic parameters: the short circuit current (J_{sc}), the open circuit voltage (V_{oc}), the fill factor (FF), and the efficiency (η). For 30 QDs we found an efficiency around 10% more than that the ref [40]. As noticed, the increase of the number of

QDs layers in the intrinsic region of the InGaAs middle cell implies an increase of the short circuit current as well as of the efficiency owing to the additional electron-hole pairs photo-generated by the absorption of lower energy photons in the middle cell as illustrated by the EQE response. The open circuit voltage decreases slightly (approximately 30 mV). This decrease can be attributed to interface recombination in the middle cell. Relative enhancements of 30.35 % on the short circuit current and 22.58 % on the efficiency are obtained when comparing InGaP/InGaAs/Ge 3-J cell structure without and with 30 QD layers.

Fig. 7 plots the power density-voltage P-V characteristic of different InGaP/GaAs/Ge 3-J cells in same conditions as above. The power density increases with the increase of the number of QDs layers and some kind of saturation appears when comparing 20 and 30 QD layer cell structures. A maximal power density of about 39.03 mW/cm^2 is achieved for 30 pairs of $In_{0.70}Ga_{0.30}As$ (QD)/GaAs (barrier). Between a solar cell 3-J and a solar cell 3-J which contains 30xQDs, a relative efficacity gain equal to 18% is obtained.

Fig. 8 shows the effect of the quantum dot number inserted in the multi-junction solar cell $In_{0.60}Ga_{0.40}P/In_{0.17}Ga_{0.83}As/Ge$ on the density of the short circuit current and the open circuit voltage. We varied the number of quantum dots (QDs) from 0 to 30. The increase of the inserted QDs number causes a considerable increase in the current density from 15.30 to $20mA/cm^2$, that is to say there is a gain of $\delta j_{sc} = 4.70mA/cm^2$. When the number of QDs exceeds 30, the current density and the open circuit voltage do not become constant. Inserting a number of QDs decreases the open circuit voltage. The V_{oc} voltage decreases from 2.35 to 2.30V. An open circuit voltage loss of $\delta V_{oc} = 0.05V$ is detected. The impact of incorporating a number of QDs on the open circuit voltage is opposite to that of the current density. It can be seen that the effect of the QDs number on the open circuit voltage is small compared to the current density.

Fig. 9 shows the effect of QDs number on the efficiency and the form factor. The increase in the QDs number induces an increase in efficiency and a decrease in fill factor. When we increase the QDs number from 0 to 30, the efficiency increases from 31.84% to 39.03%, that is to say we gain 7.19% of efficiency. On the other hand, increasing the QDs number decreases the form factor from 88.20% to 81.70%, that is to say, a loss of δFF=6.50%. This simulation allows us to optimize the performance of the proposed solar cell. Our goal is to optimize the triple junction cell; we set the indium concentration (In) in the two structures InGaP and InGaAs in order to have a multijunction solar cell. Also, we have optimized the QDs number to increase the absorption and efficiency of the studied solar cell.

Fig. 10 displays the capacitance density-voltage C-V characteristic of InGaP/InGaAs/Ge 3-J structure without and with 30 QDs layers calculated for different frequencies (1 kHz, 500 kHz, and 1 MHz). At low frequency (1 kHz), it can be seen that the capacitance density without and with 30 QDs shows the same behavior with increasing bias voltage, reaching a maximum at the forward turn-on voltage (curling point on the C-V curve). Beyond this turn-on voltage, the capacitance density decreases due to the increase of radiative recombination phenomenon and the device operates as an electroluminescent diode. Moreover, it is clear that the forward turn-on voltage of the structure without QDs layers is higher than that of structure with QDs layers, indicating that the open circuit voltage, V_{oc}, of a 3-J solar cell without QDs is higher than that of a 3-J solar cell with QDs. Otherwise, at higher frequencies (500 kHz and 1 MHz), the capacitance density starts decreasing at 1.9 to 2.1V for structure with and without 30 QDs and exhibits a slight increase at roughly 2.3-2.35V for both structures. Those C-V results show that the rate of non-radiative recombination is higher in 3-J solar cell including QDs layers and, thus, they present relatively high number of interfacial states.

4. CONCLUSION

In this paper, InGaP/InGaAs/Ge 3-J without and with QDs layers inserted in the InGaAs middle cell was simulated and optimized. It was found that the insertion of 30 $In_{0.70}Ga_{0.30}As$/GaAs QDs layers improves the EQE of middle cell in the 900-1000 nm wavelength range by a relative enhancement of about 13%. In the same conditions, the efficiency of the 3-J cell was increased from 31.84 to 39.03 %; leading to a relative enhancement of about 18%. C-V modeling shows that the lower open circuit voltage that is obtained for QDs based cell is due to interface carrier recombination in the middle cell. Insertion of $In_{0.70}Ga_{0.30}As$ QDs can so enhance the efficiency of solar cells. This study can be improved by using other materials such as quaternary semiconductors III.V-N.

References

[1] O. Amiri, N. Mir, F. Ansari, M. Salavati-Niasari, Design and fabrication of a high performance inorganic tandem solar cell with 11.5% conversion efficiency, Electrochimica Acta 252 (2017) 315–321.

[2] S. Sharbati, I.Gharibshahian, A.A. Orouji, Proposed suitable electron reflector layer materials for thin-film $CuIn_{1-x}Ga_xSe_2$ solar cells. Opt. Mater. 75, (2018), 216–223

[3] T. Kato, J-L.Wu, Y. Hirai, H. Sugimoto, and V. Bermudez,. Record efficiency for thin film polycrystalline solar cells up to 22.9% achieved by Cs-treated Cu (In, Ga) $(Se, S)_2$. IEEE J. Photovoltaic. 9, (2019), 325–330.

[4] H. Safajou, H. Khojasteh, M. Salavati-Niasari, S. Mortazavi-Derazkola, Enhanced photocatalytic degradation of dyes over graphene/Pd/TiO_2 nanocomposites: TiO_2 nanowires versus TiO_2 nanoparticles, Journal of Colloid and Interface Science 498, (2017),423–432.

[5] B. Tian , X. Zheng, TJ. Kempa , Y. Fang , N. Yu , G. Yu , J. Huang , CM. Lieber, Coaxial silicon nanowires as solar cells and nanoelectronic power sources. Nature. , 18;449(7164), (2007), 885-9

[6] H. Cotal, C. Fetzer, J. Boisvert, G. Kinsey, R. King, P. Hebert, H. Yoon and N. Karam, III–V multijunction solar cells for concentrating photovoltaics, Energy Environ. Sci., 2, (2009), 174–192

[7] K. Tanabe, A review of ultrahigh efficiency III-V semiconductor compound solar cells: multijunction tandem, lower dimensional, photonic up/down conversion and plasmonic nanometallic structures. Energies 2(3), (2009), 695–696.

[8] R. Bestam, A.Aissat, J. P. Vilcot, High efficiency quadruple junction solar cells, Superlattices an Microstructures, Volume 91(2016) 22-30

[9] A. Luque, A. Marti, Increasing the efficiency of ideal solar cells by photon induced transitions at intermediate levels. Physical Review Letters 78: (1997), 5014–5017.

[10] N. J. Ekins-Daukes, D. B. Bushnell, J. P. Connolly, K. W. J. Barnham, M. Mazzer, J. S. Roberts, G. Hill, and R. Airey, "Strain-balanced quantum well solar cells," Physica E, vol. 14, (2002), 132–135,.

[11] F. W. Ragay, J. H. Wolter, A. Marti, and G. L. Araujo, "Experimental analysis of GaAs-InGaAs MQW solar cells," in Proc. IEEE First World Conf. Photovoltaic Energy Convers., Dec. 5–9, (1994), 1754–1759.

[12] P. Kailuweit, R. Kellenbenz, S. P. Philipps, W. Guter, A. W. Bett, and F. Dimroth, "Numerical simulation and modeling of GaAs quantum-well solar cells," J. Appl. Phys., vol. 107, no. 6, (2010), 064317-1–064317-6.

[13] R. B. Laghumavarapu, A. Moscho, A. Khoshakhlagh, M. El-Emawy, L. F. Lester, and D. L. Huffaker, "Improved device performance of InAs/GaAs quantum dot solar cells with GaP strain compensation layers,Appl. Phys. Lett., vol. 91, (2007), 243115-243115-6.

[14] D. Guimard, R. Morihara, D. Bordel, K. Tanabe, Y. Wakayama, M. Nishioka, and Y. Arakawa, "Fabrication of InAs/GaAs quantum dot solar cells with enhanced photocurrent and without degradation of open circuit voltage," Appl. Phys. Lett., vol. 96, no. 20, (2010), 203507-1–203507-3.

[15] G. Jolley, H. F. Lu, L. Fu, H. H. Tan, and C. Jagadish, "Electron-hole recombination properties of $In_{0.5}Ga_{0.5}$ As/GaAs quantum dot solar cells and the influence on the open circuit voltage," Appl. Phys. Lett., vol. 97, (2010), 123505-1–123505-3.

[16] K. A. Sablon, J. W. Little, V. Mitin, A. Sergeev, N. Vagidov, and K. Reinhardt, "Strong enhancement of solar cell efficiency due to quantum dots with built-in charge," NanoLett., vol. 11, (2011), 2311–2317.

[17] C. G. Bailey, D. V. Forbes, R. P. Raffaelle, and S. M. Hubbard, "Near 1 V open circuit voltage InAs/GaAs quantum dot solar cells," Appl. Phys. Lett., vol. 98, no. 16, (2011), 163105-1–163105-3.

[18] D. Zhou, P. E. Vullum, G. Sharma, S. F. Thomassen, R. Holmestad, T. W. Reenaas, and B. O. Fimland, "Positioning effects on quantum dot solar cells grown by molecular beam epitaxy," Appl. Phys. Lett., vol. 96, no. 8, (2010), 083108-1–083108-3.

[19] A.-B.A.Mohamed, H.Eleuch, C.H.Raymond Ooi, Quantum coherence and entanglement partitions for two driven quantum dots inside a coherent micro cavity, Physics Letters A, Volume 383, Issue 29, 15 (2019), 125905.

[20] CY. Ngo, SF. Yoon, WK. Loke, TK. Ng, SJ. Chua, Photovoltaic characteristics of InAs/InGaAs/GaAs QD heterostructures. Journal of Crystal Growth; 311: (2009),1885–1888.

[21] CG. Bailey, SM. Hubbard, DV. Forbes, RP. Raffaele, Evaluation of train balancing layer thickness for InAs/GaAs quantum dot arrays using high resolution X-ray diffraction and photoluminescence. Applied Physics Letters, 95, (2009), 203100–13.

[22] J. Zribi, B. Paquette, A. Turala, A. Boucherif, B.Ilahi, A. Jaouad, V. Aimez, D. Morris, R. Arès, O. Theriault, and K. Hinzer. International Conference on Concentrator Photovoltaic Systems, April 15-17, Miyazaki, Japan 2013.

[23] Stephen M. Ramey and Rahim Khoie, Modeling of Multiple-Quantum-Well Solar Cells Including Capture, Escape, and Recombination of Photoexcited Carriers in Quantum Wells, IEEE Transactions on Electron Devices, VOL. 50, NO. 5, (2003), 1179- 1188

[24] F. Benyettou, A. Aissat, M. Benamar, J. Vilcot, Electrical properties of InAsP/Si quantum dot solar cell, International Journal of Hydrogen Energy. 42, (2017), 19512.

[25] Y. Huang, S. Aharon, A. Rolland, L. Pedesseau, O. Durand, L. Etgar, and J. Even. Influence of Schottky contact on the C-V and J-V characteristics of HTM-free perovskite solar cells. EPJ Photovoltaics; 8: (2017), 85501.

[26] DJ. Roulston, ND. Arora, and SG. Chamberlain. Modeling and Measurement of Minority-Carrier Lifetime versus Doping in Diffused Layers of n /p Silicon Diodes. IEEE Trans on Electron Devices Feb ED-29: (1982), 284-291.

[27] M. J. Hargrove, A. K. Henning, J. A. Slinkman, C. E. Hembree, Thayer School of Engineering, Dartmouth College : Technical Report, 1998.

[28] T. Olivier. Analysis of the external quantum efficiency of quantum dot-enhanced multijunction solar cells. Phd Thesis. University of Ottawa; 2015.

[29] C. I. Cabrera, J. C. Rimada, J. P. Connolly, and L. Hernandez. Modelling of GaAsP/InGaAs/GaAs strain-balanced multiple-quantum well solar cells. Applied Physics Letters, 113: (2013), 024512.

[30] G. Bastard, Wave Mechanics Applied to Semiconductor Heterostructures, Physics Editions, Paris, France, 1988.

[31] A. Aissat, R. Bestam, B. Alshehri, J.P. Vilcot, Modeling of the absorption properties of $Ga_{1-x}In_xAs_{1-y}N_y$/GaAs quantum well structures for photodetection applications, Superlattices and Microstructures,Volume 82, (2015), 623-629.

[32] M. Courel , J. C. Rimada and L. Hernández, GaAs/GaInNAs quantum well and superlattice solar cell, Applied Physics Letters 100, (2012) 073508.

[33] A. H. Reshak, Oleg. V. Parasyuk, H. Kamarudin, I. V. Kityk, Zeyad A. Alahmed,Nasser S. AlZayed, Sushil Auluck, Anatolii O. Fedorchukh and J. Chyskýi. Experimental and theoretical study of the electronic structure and optical spectral features of $PbIn_6Te_{10}$. RSC adv (2016), 77.

[34] I. Vurgaftman, J. R. Meyer, and L. R. Ram-Mohan, Band parameters for III–V compound semiconductors and their alloys, Journal of Applied Physics Volume 89, Number 11, (2001) 5815- 5875.

[35] S. Adachi, Physical properties of III-V semiconductor compounds : InP, InAs, GaAs, GaP, InGaAs, and InGaAsP, Published in New York by Wiley, 1992.

[36] H J Hovel; Robert K Willardson; Albert C Beer,Semiconductors and semimetals. Vol. 11, Solar cells, New York : Academic Press, 1975.

[37] H. Mathieu, P. Lefebvre, and P. Christol, Simple analytical method for calculating exciton binding energies in semiconductor quantum wells, PhysicaL Review B, Volume 46, Number 7, (1992) 4092- 4101.

[38] F. Benyettou , A .Aissat, M .Benamar, and J. P. Vilcot Modeling and Simulation of GaSb/GaAs Quantum Dot for Solar Cell. Energy Procedia; 74: (2015), 139.

[39] J. Piprek, Semiconductor Optoelectronic Devices: Introduction to Physics and Simulation. UCSB: Academic Press (2003), 22.

[40] M. A. Green, K. Emery, Y. Hishikawa, W. Warta and E. D. Dunlop, "Solar cell efficiency tables, Prog. Photovoltaics, Res. Appl., vol. 22, (2014), 701–710.

Figures captions

Fig.1. Structure of solar celle triple junction.

Fig.2 . a) Structure of InGaP/InGaAs/Ge 3-J with 20 InGaAs(QD)/GaAs(barrier) layers inserted in InGaAs middle cell, b) structure of the midlle solar cell with insertion of QDs based on InGaAs/GaAs.

Fig.3. Current density of InGaP/InGaAs/Ge 3-J as function of voltage.

Fig. 4. Power density of InGaP/InGaAs/Ge 3-J as function of voltage.

Fig. 5. EQE response of InGaAs midlle cell without and with 30 QDs layers.

Fig. 6. J-V of InGaP/InGaAs/Ge 3-J without and with variable number of QDs layers inserted.

Fig. 7. P-V of InGaP/InGaAs/Ge without and with different number of QDs layers.

Fig. 8. Effect of QDs number on the J_{sc} and V_{oc}.

Fig. 9. Effect of QDs number on the FF and efficiency.

Fig.10. C-V of InGaP/InGaAs/Ge without and with 30 QD layers calculated at different frequencies 1 kHz, 500 kHz, and 1 MHz.

TABLE I. The parameters of the materials

TABLE II. Parameters of the 3-J solar cell without and with QD layers.

TABLE III. Electrical parameters of 3-J with and without quantum dot layers for different number of QDs.

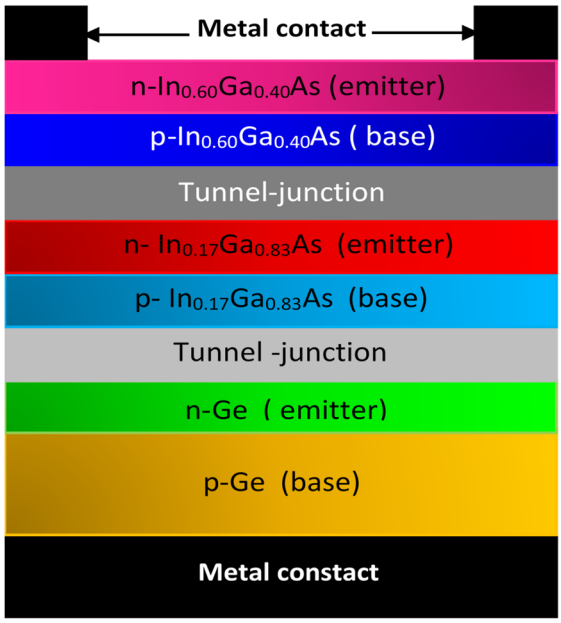

Figure. 1

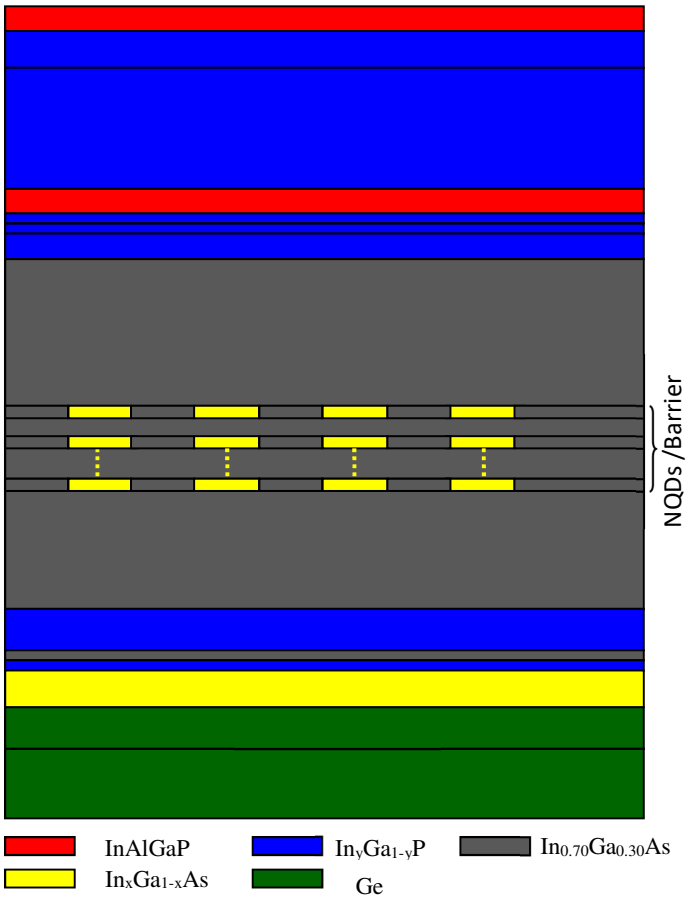

Figure. 2.a

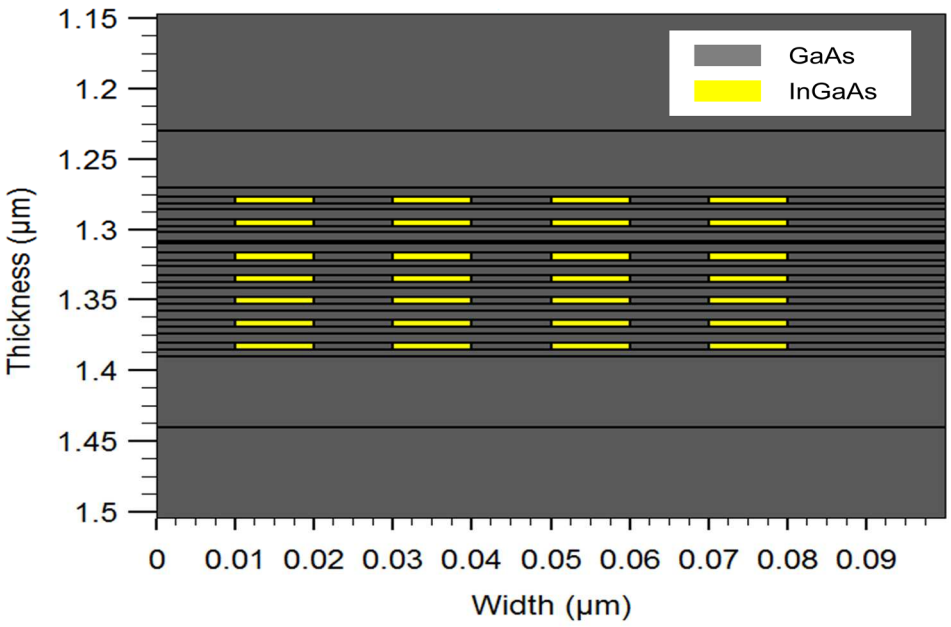
GaAs
InGaAs
Thickness (μm)
1.15
1.2
1.25
1.3
1.35
1.4
1.45
1.5
0
0.01
0.02
0.03
0.04
0.05
0.06
0.07
0.08
0.09
Width (μm)

Figure.2. b

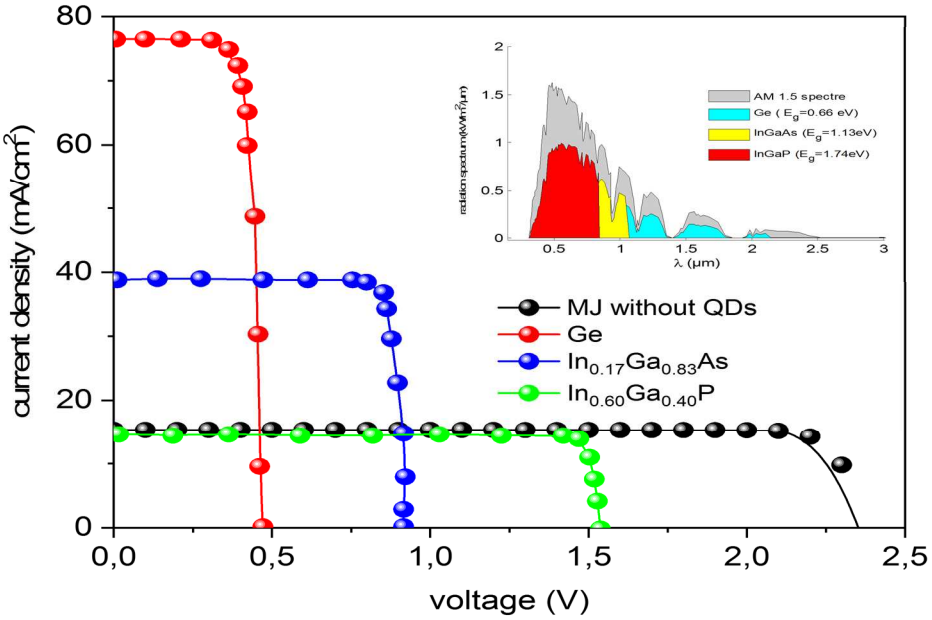

Figure .3

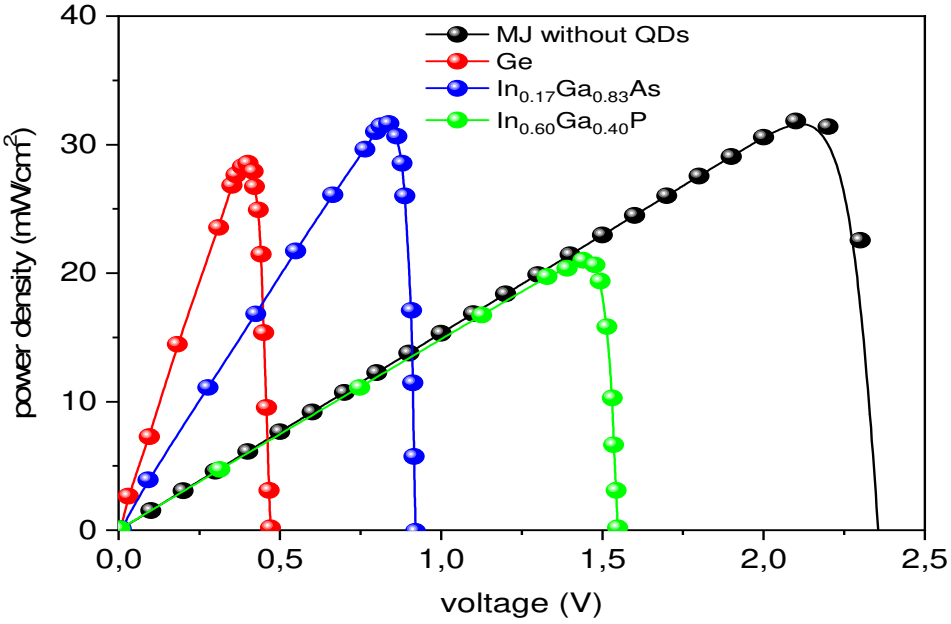

Figure .4

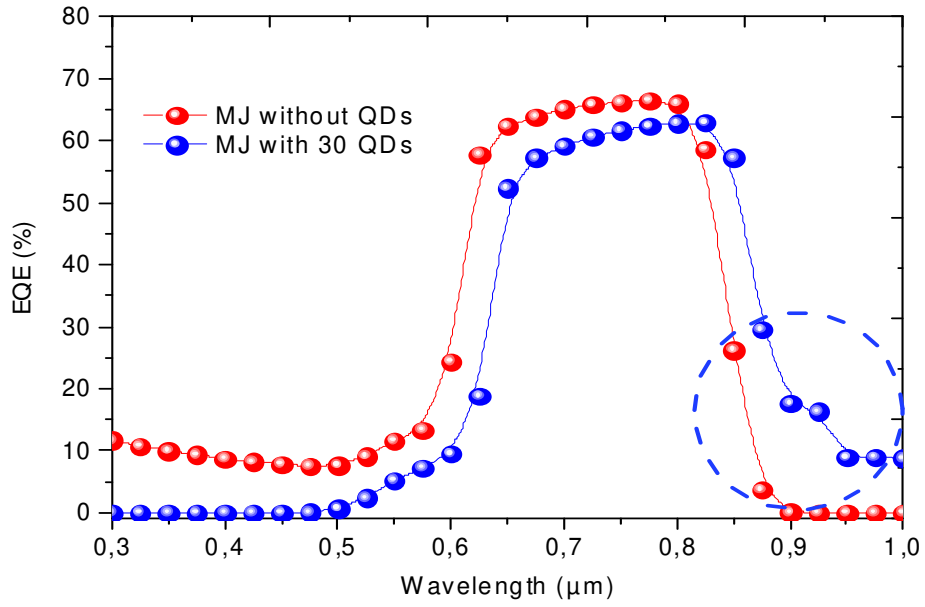

Figure. 5

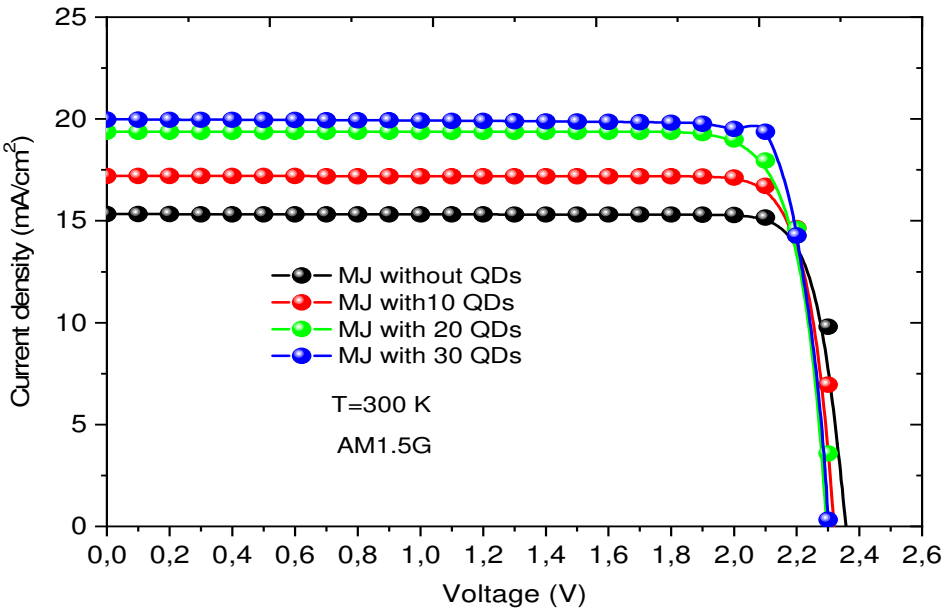

Figure 6

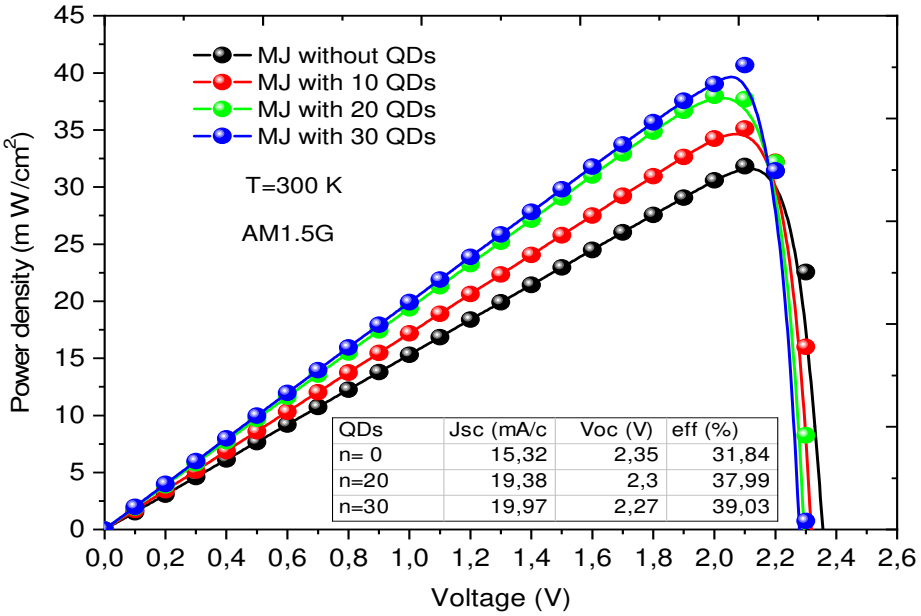

Figure. 7

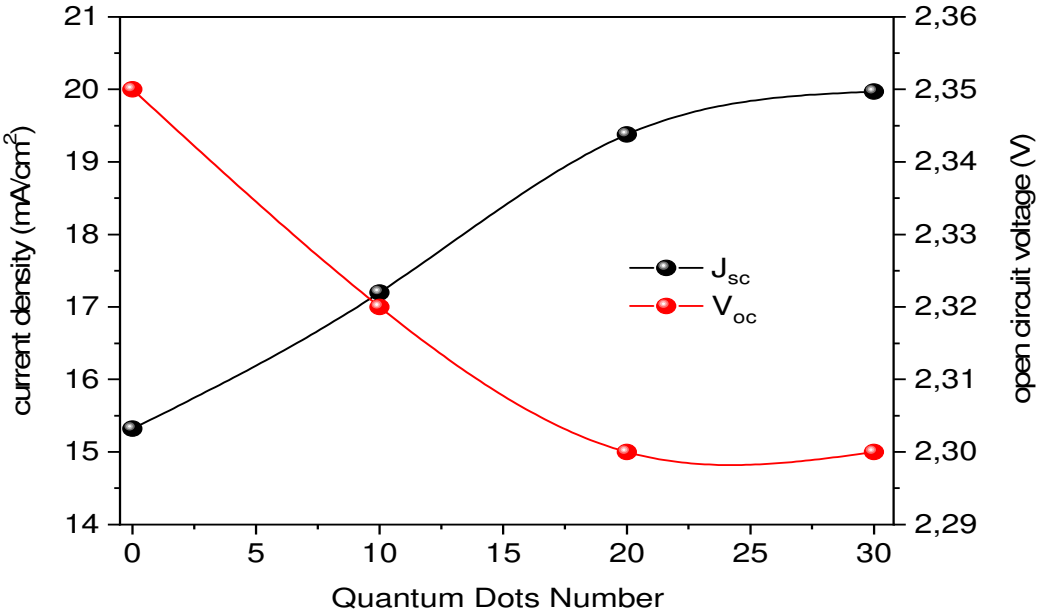

Figure.8

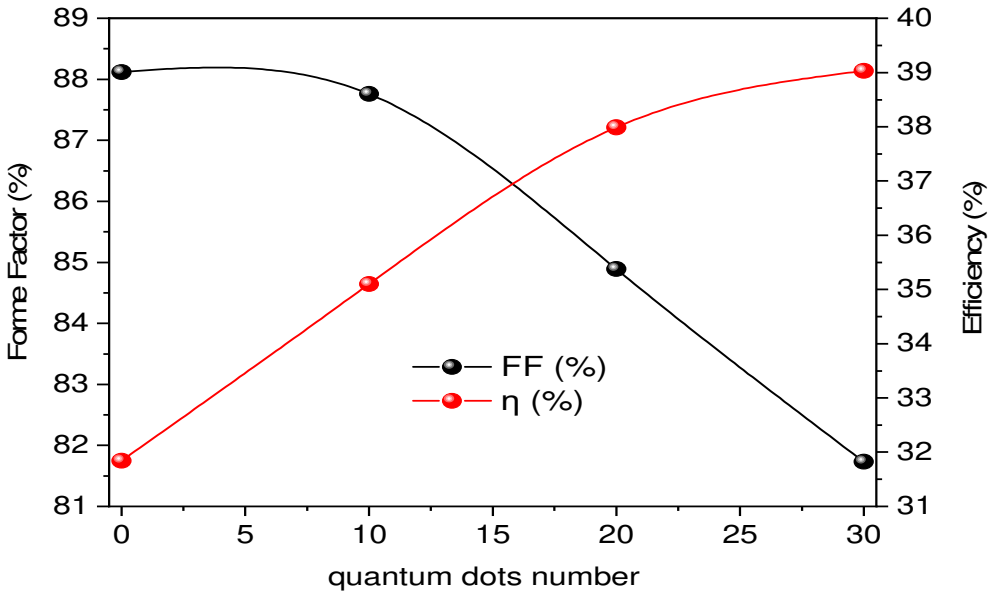

Figure .9

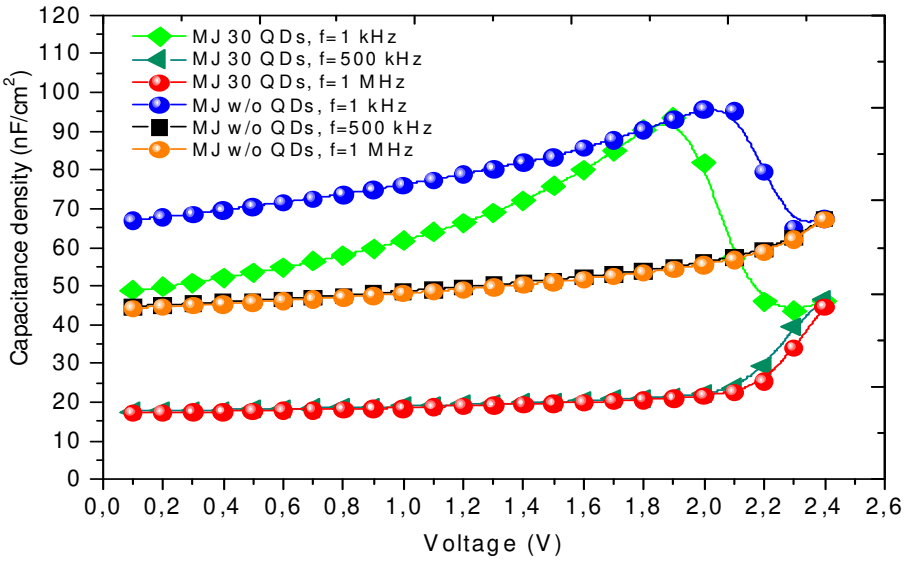

Figure. 10

Parameter	GaAs	InAs	InP	GaP
a(Å)	5.65	6.05	5.87	5.45
E_g(eV)	1.42	0.35	1.35	2.78
a_c(eV)	−7.17	−5.08	-6.0	8.20
Δ_0(eV)	0.34	0.39	0.11	0.08
a_v(eV)	1.16	1.00	-0.6	1.70
b(eV)	−1.7	−1.8	-2.0	−1.6
m_e^*	0.07	0.03	0.08	0.13
C_{11}(GPa)	1221	8.329	1011	1405
C_{12}(GPa)	566	4.526	5.61	620.3
γ_1	6.80	20.00	5.08	4.05
γ_2	1.90	8.5	161	0.49
γ_3	2.93	9.20	2.10	2.93
m_l^*	1.90	0.64	0.41	2.00
m_t^*	0.078	0.05	0.03	0.25
m_{so}^*	1.72	0.14	0.21	0.25
ε_r	13.10	14.60	12.40	11.11

Table I

Cell	Layer	Composition	Thickness (nm)	Carrier concentration(cm^{-3})
Top cell	Window	p^+-InAlGaP	30	2×10^{18}
	Emitter	p^+-InGaP	50	2×10^{18}
	Base	n-InGaP	550	7×10^{16}
	BSF	n^+-InAlGaP	30	2×10^{18}
Tunnel cell	Emitter	n^+-InGaP	15	5×10^{19}
	Base	p^+-InGaP	15	3×10^{19}
Middle cell (NxQD/Barrier)	Window	p^+-InGaP	40	3×10^{18}
	Emitter	p^+-InGaAs	500	2×10^{18}
	Barrier	GaAs	115	Undoped
	QDs	$In_{0.70}Ga_{0.30}As$	5	Undoped
	Base	n-InGaAs	2000	2×10^{17}
	BSF	n^+-InGaP	100	5×10^{18}
Tunnel cell	Emitter	n^+-GaAs	15	5×10^{19}
	Base	p^+-InGaP	15	3×10^{19}
Bottom cell	Window	p^+-InGaAs	50	5×10^{18}
	Emitter	p^+-Ge	100	2×10^{18}
	Base	n-Ge	10000	1×10^{17}

Table II

QDs Number	J_{sc} (mA/cm^2)	V_{oc} (V)	FF (%)	η (%)
0	15.32	2.35	88.12	31.84
10	17.2	2.32	87.76	35.10
20	19.38	2.30	84.89	37.99
30	19.97	2.30	81.73	39.03
Ref [42]	29.68	1.12	86.00	28.80

Table III